High-resolution numerical modelling of a marine mine tailings discharge in Western Norway

Raymond Nepstad [a,*], Maria Liste [a], Morten O. Alver [a,b], Tor Nordam [a,c], Emlyn Davies [a], Tormod Glette [d]

[a] SINTEF Ocean, Trondheim, Norway
[b] Department of Engineering Cybernetics, NTNU, Trondheim, Norway
[c] Department of Physics, NTNU, Trondheim, Norway
[d] DNV GL, Høvik, Norway

A B S T R A C T

Waste from mining operations includes mine tailings, a slurry of fine-grained mineral particles and processing chemicals that remains after the desired compounds have been extracted from the ore. In some cases, the method of disposal is to place tailings into the marine environment; this is known as Submarine Tailings Placement (STP). To understanding the environmental impact of releasing large amounts of mine tailings into the marine system, multiple processes must be well characterised, including those relating to the transport and fate of the disposed material.

We applied a set of high-resolution models for wind, hydrodynamics, and sediment transport to simulate a submarine mine tailings discharge in a Norwegian fjord. The transport model includes processes to account for the effect of flocculation on mine tailings transport and fate. We calculated the mean tailings sedimentation rate in the fjord, which is closely related to the environmental footprint of the STP. Comparisons with measurements of winds, currents, turbidity, and sedimentation rates were made to evaluate the model, and we found overall reasonable agreement. We investigated discharge scenarios during 2013 and identified a strong wind event around November 17, which caused increased particle dispersal. The increased mixing caused by the strong winds were seen in elevated turbidity measurements, as well as increased modelled suspended sediment concentration.

1. Introduction

In the process of extracting and processing ore from mining, a large quantity of fine-grained waste material is produced and must be disposed of (Kvassnes and Iversen, 2013). Among the most critical environmental issues of industrial mining is the safe disposal of these mine tailings, which in addition to fine particulates, also contain residual chemicals used during processing (Ramirez-Llodra et al., 2015). The most common approach is to use a landfill or tailings dam (Skei, 2013), which lays claim to a significant portion of land. In some cases an alternative disposal method is used, where the tailings are deposited on the ocean floor, by way of a more than 100 year old concept known as Submarine Tailings Placement (STP) (Dold and Bernhard, 2014; Ramirez-Llodra et al., 2015; Skei, 2013; Kvassnes and Iversen, 2013). In Norway there are at present several active and planned STP sites, located in fjords throughout the country (Ramirez-Llodra et al., 2015). Fjords are often highly complex systems (Aure et al., 2007), showing intricate seasonal circulation patterns (Farmer and Freeland, 1983) and productive ecosystems (Mevenkamp et al., 2017).

STPs have implication for the marine environment (see, e.g. Ramirez-Llodra et al., 2015; Morello et al., 2016; Farkas et al., 2017; Mevenkamp et al., 2017). In addition to smothering of the immediate area of the sea bed around the discharge point, tailings particulates and residual chemicals may come into suspension and be transported with ocean currents, potentially affecting both the water column and sea bed over a larger area. To minimise the potential environmental impacts, the use of an STP to dispose of tailings requires in-depth knowledge about the hydrodynamics and ecosystem at the disposal site as well as strict control of the discharge itself. Routine monitoring and scientific investigations over the past decades, and in particular in the past few years, have provided much insight into the extent of impacts and dynamics of tailings in the ocean. For some recent reports and reviews, see, e.g. Jensen and Hylland (2019), Sternal et al. (2017), Lepland et al. (2019), Davies and Nepstad (2017), Morello et al. (2016), Ramirez-Llodra et al. (2015), and references therein.
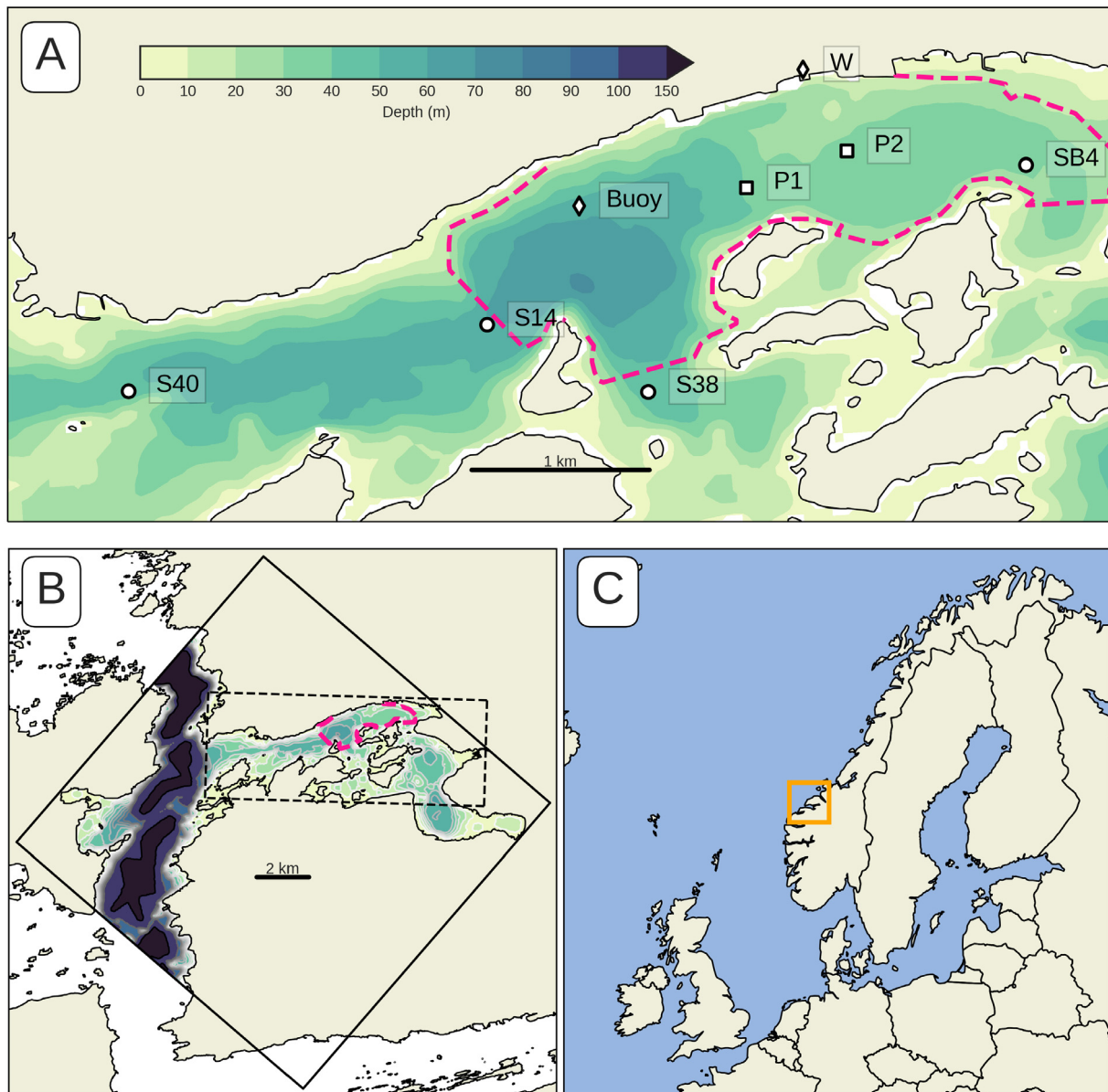
Fig. 1. Overview of model domains, the STP area (red dashed line) and sampling stations. Panel A: the location of the STP discharge points (P1 and P2) within the STP area, and named positions of sampling stations of available data. Panel B: Domain extents of the SINMOD circulation model (full black line) and the DREAM transport-fate model (dashed black line). Panel C: The location within Norway is indicated by the orange square. (For interpretation of the references to colour in this figure legend, the reader is referred to the web version of this article.)

Numerical models can constitute an important part of the toolbox for the sustainable management of STPs (Findikakis and Law, 1998; Vare et al., 2018). During planning, predictions of dispersal and sedimentation patterns and environmental impacts and risks can be used to evaluate candidate locations and optimise the discharge to achieve a minimal environmental footprint. In the operational phase, model predictions, combined with online monitoring, can be used to, e.g., evaluate the effect of changes to the discharge arrangement, and provide "early warning" of transient environmental events that can impact dispersion.

We recently developed new capabilities for an existing marine transport and fate model (DREAM, see, e.g., Rye et al., 1998, 2004, 2008; Reed and Hetland, 2002), in order to adapt it for simulations of STP discharges. This includes a new component in the model which calculates settling speed for particulate fines based on concentration to account for flocculation effects.

In this paper, we present results of numerical simulations of circulation and tailings particulate dispersal from an active STP

in Frænfjorden, Norway. Following an overview of the STP area and discharge, we summarise relevant features of the numerical models used, before simulation results are presented. Model predictions are compared with measurements of current, turbidity and sedimentation rates to assess their quality. We identify and discuss an interesting transient environmental situation, where a strong wind event causes an increase in the dispersal of tailings. Estimates for long-term tailings sedimentation rates in the fjord, which relate to the environmental footprint of the STP, are also presented and discussed.

2. Materials and methods

2.1. The tailings discharge

We studied the STP area in Frænfjorden (7.12E, 69.845N), western Norway, where a calcium carbonate processing plant has

been in operation for several decades (Omya Hustadmarmor AS), see Fig. 1. The STP area itself is defined by the publicly available discharge permit of Omya Hustadmarmor (Miljødirektoratet, 2015), and the line shown in the figure is based on data from an environmental monitoring report (Glette, 2014). The mine tailings discharge from this plant, a slurry consisting of water, residual processing chemicals (e.g. flotation chemicals) and particulates of calcium carbonate and other minerals (Ramirez-Llodra et al., 2015; Miljødirektoratet, 2015), are continuously discharged from a set of pipes at a depth of 20 m. The particulates contain a large fraction of fines ($< 20\ \mu$m), as well as larger particles with diameters extending up 800 μm. The full particle size distribution is shown in Fig. 2, and this distribution is used to set initial particle sizes in the plume model (described later). The discharge rate varies over time, as does the position of the discharge, which is switched between a western (main, 37 m water depth) pipe and an eastern (backup, 31 m water depth) pipe, placed 500–600 m apart. During November 2013, the rate fluctuated around a median value of 400 m^3/h, mainly released through the eastern pipe, as shown in Fig. 3. In this period, the dry fraction in the discharge was approximately 12% by mass; the density of the dry fraction was 2.4 tonnes/m^3. Before discharge the tailings, which contain residual processing freshwater, are mixed with seawater from the fjord, resulting in a final salinity of approximately 6 g/kg.

2.2. Study area

Frænfjorden contains several islands and sills, contributing to a complex flow pattern. The Frænfjorden inlet is a shallow area with a channel into the fjord which is about 40–45 m deep. Outside Frænfjorden there is a sill to the north and two sills to the south, which are all about 100 m deep. The bathymetry of the deposit area of the fjord is shown in Fig. 1.

The fjord has a classic estuarine circulation pattern where the surface waters flow seawards and intermediate waters flow inwards below these surface layers. The water body of the fjord is stratified in spring/summer due to the freshwater supply from several rivers and streams. The circulation is also affected by the ever-changing stratification of the adjacent waters outside the fjord, which is modified by both local and seasonal winds. As the discharge of tailings is below the surface layer, the circulation pattern in Frænfjorden causes the particles to mostly remain inside the fjord, rather than get transported seawards, unless intense vertical mixing brings the particles upwards.

2.3. Atmospheric model

Interactions between atmosphere and ocean play an essential role in the dynamics of the upper ocean, and accurately modelling these dynamics at a suitably high resolution is crucial, especially in fjord systems (Myksvoll et al., 2012). The Weather Research and Forecasting (WRF) Model (Skamarock et al., 2008) has been used to provide atmospheric data in this study. WRF is a fully compressible conservative-form non-hydrostatic atmospheric model suitable for both research and weather prediction applications. The initial data (meteorological data) and boundary conditions necessary for model initialisation are wind components, potential temperature, pressure, and moisture; all of them came from ERA-interim, a global atmospheric reanalysis going back to 1979, which is continuously updated. These global data are introduced into the model by a relaxation method (Davies and Turner, 1977). A high-resolution setup nested in three steps, 20 km, 4 km and 1.33 km horizontal resolution grids, has been used to provide atmospheric forcing (input data used in the ocean circulation model) at a mesoscale horizontal resolution of 1.33 km at one-hour sample interval.
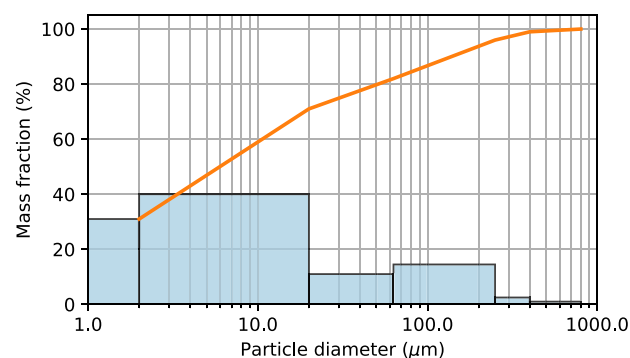

Fig. 2. Particle size distribution of discharged tailings. Orange line is the cumulative distribution.

2.4. Circulation model

The transport-fate model requires circulation and vertical diffusivity 3+1D fields as input. For this purpose, we ran the SINMOD ocean model (Slagstad and McClimans, 2005), set up with a 32 m horizontal resolution domain to properly capture the circulation properties of the STP area. The hydrodynamic model domain is shown in Fig. 1(B). SINMOD is based on the primitive Navier–Stokes equations, and uses a z-coordinate grid. The model is run in a 5-level nested setup where the outer domain covers the northern part of the Atlantic as well as the Arctic Ocean in 20 km resolution. Each nesting step increases horizontal model resolution by a factor of 5. Tidal forcing is applied on the boundaries of the outer domain, based on TPXO 7.2 (Egbert and Erofeeva, 2002), and propagates into the higher resolution domains. Eight tidal components (M2, S2, K1, N2, K2, O1, P1 and Q1) are included.

The 32 m domain covering Frænfjorden has 30 vertical z-layers, where the layer boundaries are horizontal and not terrain following. The thickness of the upper layer varies with ocean surface height, while the remaining layers have constant thicknesses ranging from 0.5 m near the surface to 25 m below a depth of 100 m. Vertical sub-grid diffusivity is calculated from winds, and from current shear and stratification using a Richardson-based scheme (Sundfjord et al., 2008).

The bathymetry of the high resolution model setup is based on a digital bathymetry model (DBM) in 25 m resolution from the Norwegian Mapping Authority (www.kartverket.no), supplemented by OLEX data (www.olex.no). For the large scale setups, the IBCAO (Jakobsson et al., 2012) and ETOPO (Amante and Eakins, 2009) data sets are used along with the DBM. River run-off is included at all nesting levels, and in the 32 m domain the following rivers were included: Storelva, Malmelva, Aureelva, Eikremselva, Sylteelva, Torneselva and Myrbostadelva. The discharge rates of these rivers were based on average annual precipitation data from NVE (The Norwegian Water Resources and Energy Directorate). In addition we specified a diffuse runoff (along land, between rivers) of 1.8 m^3/s according to mean freshwater runoff from land to sea (data from NVE Atlas[1]). Diffuse runoff was used for the northern side of the fjord only, as the drainage area here is larger than the drainage area to the southern side of the fjord.

2.5. Transport and fate model

The transport and fate model (DREAM, Rye et al., 1998, 2004, 2008) is based on a Lagrangian particle formulation of the

---

[1] http://atlas.nve.no/html5Viewer/?viewer=nveatlas.
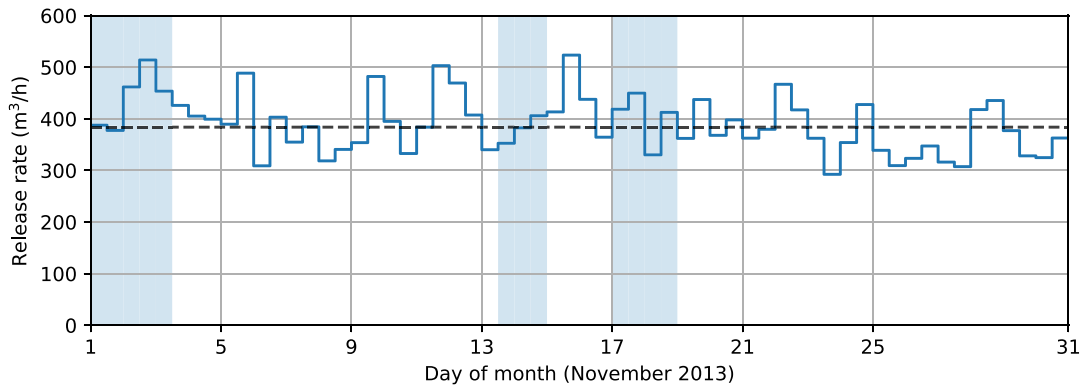
Fig. 3. Total tailings discharge rate for November 2013 (12 h mean values), and median discharge rate (dashed line). The shaded regions indicate discharge from the western pipe, otherwise discharge from the eastern pipe.

advection–diffusion–reaction equation (see e.g. van Sebille et al., 2018 for a recent review of Lagrangian methods in oceanography). Briefly, a particulate discharge, such as mine tailings, is partitioned into discrete parcels (numerical particles), which are assigned a set of physical properties and tracked through the water column as they move due to advection, turbulent diffusion and settling. Upon release, each numerical particle is assigned a physical particle size, drawn from the given distribution (see Fig. 2), such that each numerical particle represents a certain mass of physical particles with that size. Physical concentrations are calculated from the particle position and masses on a regular 3D grid, using a kernel density estimation method with cylindrical kernels (Reed and Hetland, 2002). Particles reaching the sea bed through settling will deposit mass onto an auxiliary sediment grid.

Upon initial discharge the mine tailings slurry forms a negatively buoyant plume, which descends through the water column, entraining ambient sea water in the process, diluting the plume and lowering its density. This phase is described by a Lagrangian plume model (Lee and Cheung, 1990; Johansen, 2000), coupled to the main transport-fate model. The plume is modelled as a series of elements, where each element has the shape of a conical frustum. The width of the plume increases along its length, to account for the volume of entrained water. The ambient currents are taken into account in a one-way offline coupling from the current model to the plume-model, with the current affecting the trajectory of the plume, and the rate of forced entrainment. An example of predicted plume trajectories and radii from the present simulations are shown in Fig. 4, where the plume descends to the sea bed and terminates there.

Numerical particles that are inside the plume have a position that follows the centreline of the plume, with an added random displacement given by the radius of the plume at that point. A particle can leave the plume either by falling out of the plume due to high settling speed, or when the plume terminates. The probability of a negatively buoyant particle falling out of the plume is calculated from its settling velocity (Rye et al., 2008), such that larger or denser particles have a higher probability of leaving the plume. When the plume terminates, the particles are released into the far-field model from their last positions in the plume. The plume phase terminates either through loss of buoyancy (trapping), surfacing, or bottoming. The latter is the relevant scenario for the discharge parameters and environmental conditions considered here, where the plume has sufficient density to reach the sea bed. Once the plume terminates on the sea bed, the Lagrangian particles are released into the free water masses. The residual momentum of the plume is added to the ambient current used in the far-field model as a radially emanating component, approximating the radial wall jet that may

form in such cases (Chowdhury and Testik, 2014). For additional details on the plume model, see Johansen and Durgut (2006).

2.6. Flocculation-enhanced settling

Due to the small particle sizes and high initial concentration, the mine tailings will tend to flocculate in sea water, which consequently changes the settling speed and transport potential of the tailings (Hill et al., 2000; Skei and Syvitski, 2013). To account for this process, we implemented a concentration-dependent settling model inspired by previous work and models (Krone, 1963; Huang et al., 2006). We use a hybrid scheme, where the total suspended solid concentration is calculated from the Lagrangian particles on an Eulerian grid. These concentrations are then used to update the settling speeds of the Lagrangian particles. The steps in the model are these:

1. Calculate cell concentrations, C_{ijk} (units g/L), on an Eulerian three-dimensional grid using cylindrical kernels (see Section 2.5).
2. In each grid cell ijk, the median settling speed $\overline{w}_{ijk}$ (m/s) is given by Huang et al. (2006),

$$\overline{w}_{ijk} = b \left(\frac{C_{ijk}}{C_0} \right)^n, \quad C_0 = 1 \text{ g/L}. \tag{1}$$

where the empirical parameters b and n are described in detail below.

3. All Lagrangian particles in cell ijk draw a settling speed w from a log-normal distribution with median given by the previous step (cell index subscripts omitted here) (Neumeier et al., 2008)

$$f(w) \propto \frac{1}{w} \left[\frac{(\log w - \mu)^2}{2\sigma^2} \right], \tag{2}$$

where $\mu = \log \overline{w}$, and σ is a user-specified scale parameter, determining the width of the distribution.

4. If the new settling speed is smaller than the existing settling speed of the Lagrangian particle, it is discarded (no de-flocculation).
5. The new settling speed is assigned with a probability

$$P_{floc}(\Delta t) = 1 - 2^{-\frac{\Delta t}{\tau_s}}, \tag{3}$$

where Δt is the model timestep, and τ_s is a time scale parameter described below.

We note that all numerical particles may have their settling speeds updated as part of the flocculation-enhanced settling model. However those numerical particles that represent larger physical particles are less likely to be affected, due to their
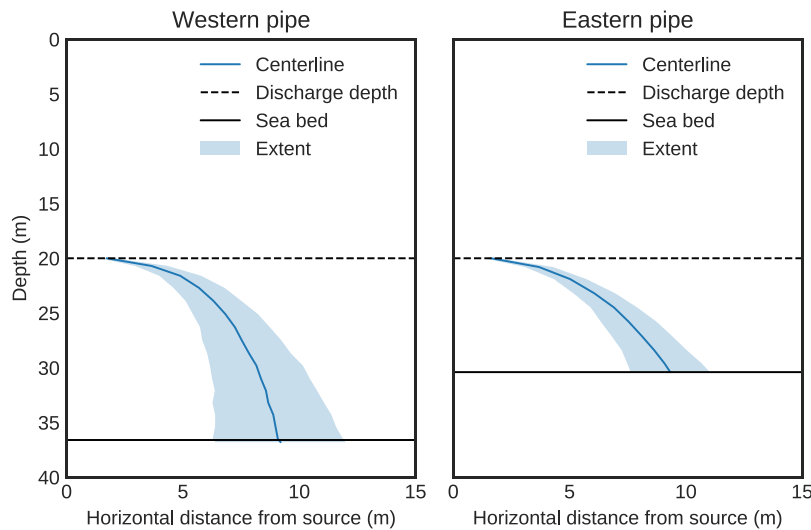
Fig. 4. Example of plume model predictions for the descending plume, shown for the two different discharge pipes. The centreline of the plume is indicated (full blue lines), as well as the radius of the plume (light blue areas). The water depth (sea bed) is indicated by the full black horizontal lines, while the dashed black vertical lines indicate the discharge depths.

initially higher settling speeds (see Steps 4 and 5 above). Hence, the main effect of the flocculation-enhanced settling model is to increase the settling speed of the smallest particles, as these would otherwise stay suspended almost indefinitely.

The "time scale" parameter τ_s ensures that flocculation is not an instantaneous process and removes dependence on the model time step. We introduce a dimensionless user-specified length scale parameter L and use it to calculate τ_s

$$\tau_s = L \frac{\overline{d}}{\overline{w}} \qquad (4)$$

The value of L defines how many median diameters $\overline{d}$ a floc may travel at the median settling speed before having a 50% chance of undergoing flocculation (Eq. (3)).

The values of b and n may be estimated from field or lab measurements of median settling speed versus concentration (e.g. Dyer, 1989), while σ and L are less directly tied to measurable quantities, but reasonable values can be determined from numerical experiments. For the present simulation we used values obtained from Kaolinite data (Dyer, 1989) as our starting point, and based on numerical experimentation settled on the final values of $b = 4 \times 10^{-5}$, $n = 0.7$, $\sigma = 4$, $L = 5000$. While these values were found to give reasonable results, it is possible that a better set of values could be found. However, a full exploration of this model for flocculation-enhanced settling is outside the scope of this investigation.

While very simple, and neglecting the many processes and actual dynamics of the flocculation process, the model can provide the approximate overall effect of flocculation on modified settling speeds of individual particles. We are mainly concerned with providing corrections to the settling speed of the finest particles in the tailings discharge in the transport-fate model, through self-aggregation. These fines can quickly form small, dense and strongly bound flocculi, which are not easily broken, and have a significantly higher settling speed than the primary particles they form from (see e.g. Lee et al., 2012). Thus we do not account for the formation and behaviour of larger, more complex flocs. Such complex flocs have been observed in Frænfjorden, but were estimated to comprise a relatively small fraction of the total discharge (Davies and Nepstad, 2017).

At present, floc breakup (leading to a reduction in settling speed) is not included in the model. Floc breakup can occur if a floc encounters a region of increased turbulence, and could in

Table 1
Positions, depth and water depth for the measurement stations.

| Station	Longitude	Latitude	Station depth (m)	Water depth (m)
SB4	7.1458	62.8446	33	35
S38	7.1051	62.8341	30	48
S14	7.0868	62.8371	30	60
S40	7.047	62.8332	49	50
RTbuoy	7.0965	62.8433	0–40	40

principle be accounted for by including a term containing the turbulent energy dissipation rate in the formula for median settling speed (see e.g. Huang et al., 2006; van Leussen, 1994). However, the smallest, strongly bound flocs that we primarily describe in model are unlikely to be broken up in this manner, assuming the Kolmogorov length scale (η) sets a limit for floc breakup. For such small flocs, the required turbulent energy dissipation rate would need to be on the order of $\epsilon = \nu^3/\eta^4 \approx 1.6$ W/kg ($\nu = 1.6 \times 10^{-6}$ m^2/s, $\eta = 40 \times 10^{-6}$ m), which is not likely to occur within the fjord.

2.7. Measurements of currents, turbidity and tailings sedimentation

An existing dataset was used to evaluate the model predictions, based on measurements performed by DNV GL (www.dnvgl.com) during 2013 and 2014 (Glette, 2014). Current and turbidity data at 4 different stations (3 on the border of the deposit area plus a reference station) were measured during a one year period (March 2013 to March 2014). In addition, sediment traps (KC-trap, 4 × 72 mm diameter tubes) were deployed 2 m above the sea bed at all stations. The current meters used were 400 kHz and 600 kHz profiling ADCPs with a sampling rate of 10 min, and each measurement averaged over 60 s. Turbidity data were collected by using Aquatec 210TTY sensors with wipers, set to 8 samples every 10 min. The proportion of limestone in the sediment from the sediment traps were measured and calculated at Omya Hustadmarmor's laboratory. Positions and depths of all stations are summarised in Table 1, and shown on the map in Fig. 1.

2.8. Simulation scenarios

We simulated a continuous, variable-rate discharge of tailings for November 2013, and we compared predicted concentrations
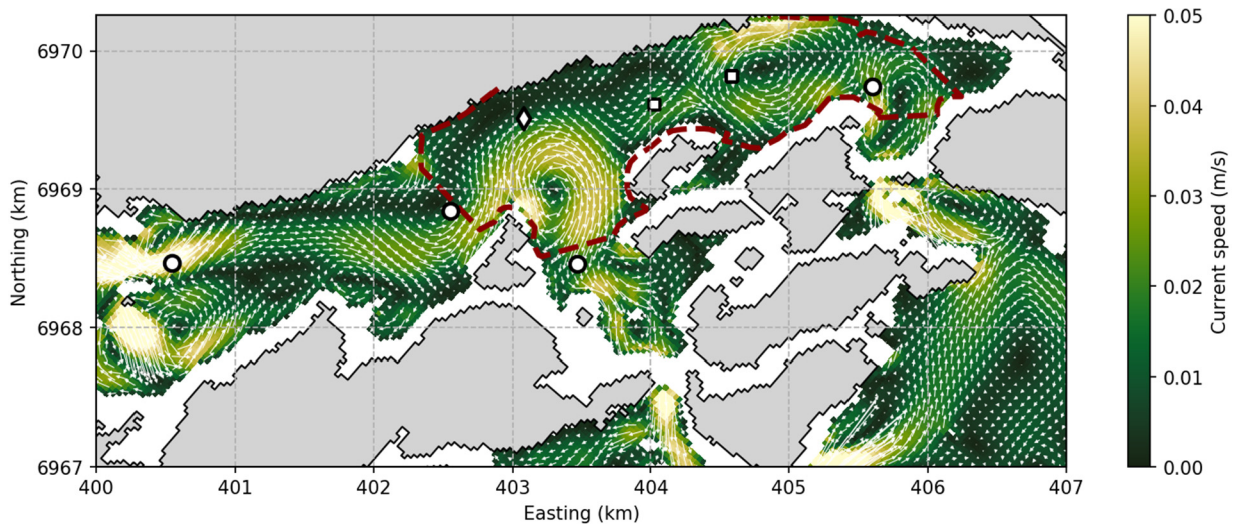
Fig. 5. Monthly mean current for November 2013, at 20 m depth. The dashed red line shows the STP area, while the white squares indicate the discharge points. The white circles and diamond are the station positions described previously.

of suspended tailings with measured turbidity during that period. We also performed a longer (6 month) simulation to investigate deposition patterns of tailings on the sea bed, and compared it with measured deposition rates. The transport model was forced with currents and vertical diffusivity output from the ocean model, and a constant horizontal diffusivity of 0.01 m^2/s was used. The model time step was 5 min, with output of the model state every 20 min. Each time step 2000 Lagrangian particles were released, and the maximum amount of particles was set to 100 000. Particles are removed when they leave the model domain through sedimentation or horizontal advection. The auxiliary grids used in the transport model was set up with 30 m horizontal resolution and 2 m vertical resolution.

3. Results and discussion

3.1. Frænfjorden circulation

Measurements and previous modelling studies in Frænfjorden (Glette, 2014; Alver et al., 2016) indicate that currents are strongest and most homogeneous in the outer part of the fjord, with mean current speeds of 12 cm/s and maximum peaks up to 55 cm/s in the east/west direction. Further inside the fjord, the current speeds decrease (mean current speeds of 7 cm/s) and is affected by the bathymetry, with the main direction changing to northeast/southwest. The inner part of the fjord has mean current speeds less than 5 cm/s. Here, the current direction is less homogeneous with both daily and periodical variations.

The predicted current at the depth of the discharge pipes (20 m depth), averaged over one month (November 2013) is shown in Fig. 5. Outside the STP area to the west, the monthly mean current is predominantly inwards in this period (and depth) while to the east and southeast the monthly mean current is mainly oriented seawards. Some hydrodynamic features are observed, notably two residual eddies located west and east of the STP area. An anticyclonic eddy over the western and deepest STP area is seen, as well as a cyclonic eddy over the shallower eastern part of the STP area, around the eastern discharge point. These features are generated by the combination of the effects of the flow direction, tide, wind forcing, and bathymetric steering. Other smaller eddies can be found in other locations outside the STP area, and their orientation and size vary accordingly. These eddies are also present in other months during the year and are likely to have a significant impact on the dispersion and distribution

of tailings in the fjord, because particles can get trapped in the re-circulation, and be retained in the STP area for a longer time.

3.2. Wind predictions and measurements

In the middle and the end of November 2013, two strong wind events occurred over the STP area in Frænfjorden (see panel B in Fig. 6). In both strong wind events, the measured wind speeds exceeded 20 m/s with maximum winds reaching 24 m/s. The modelled winds replicated the same pattern as the observed winds, but they showed a smaller magnitude with maximum winds reaching 15 m/s. The highest wind speeds are correlated with westerly, southwesterly and easterly wind directions (see panel A in Fig. 6).

Panel C in Fig. 6 shows temporal and vertical variations of the modelled water column vertical eddy diffusivity magnitude. During November 2013, diffusivities ranging from 10^{-5} m^2/s to 10^{-1} m^2/s are seen. Two significant increases in vertical diffusivity during November coincided with the highest wind speeds, but only during one of these events (November 15–18) did the vertical diffusivity change significantly throughout the water column. During November 15–18, the winds had a variable heading starting from 225° (coming from the south-west), rotating clockwise to 270° and then back counterclockwise to 225° and 90° to conclude the event. During this time, the wind speeds increased from approximately 5 m/s to near 24 m/s, then reduced to approximately 3 m/s again. Modelled vertical diffusivity varied from 5×10^{-5} m^2/s to 10^{-2} m^2/s throughout most of water column, reaching 10^{-1} m^2/s in the upper 5–7 m.

During the second wind event (November 25–29) wind speeds also increased significantly from approximately 5 m/s to near 24 m/s, then reduced to approximately 5 m/s, but wind directions were mainly from the east (90°) during the highest winds, later from the southeast (135°). During this event, modelled vertical diffusivity again varied from 5×10^{-5} m^2/s to 10^{-1} m^2/s, but only in the upper 5–7 m of the water column. Therefore, westerly and southwesterly winds in combination with high wind speeds were able to significantly increase vertical diffusion values throughout most of the water column during November 2013. By inspecting the map in Fig. 1(A), it is apparent that the fetch length is largest in the west-southwest direction, and more limited in all other directions. Hence, we expect winds from west-southwest to generate larger waves than winds from other directions.
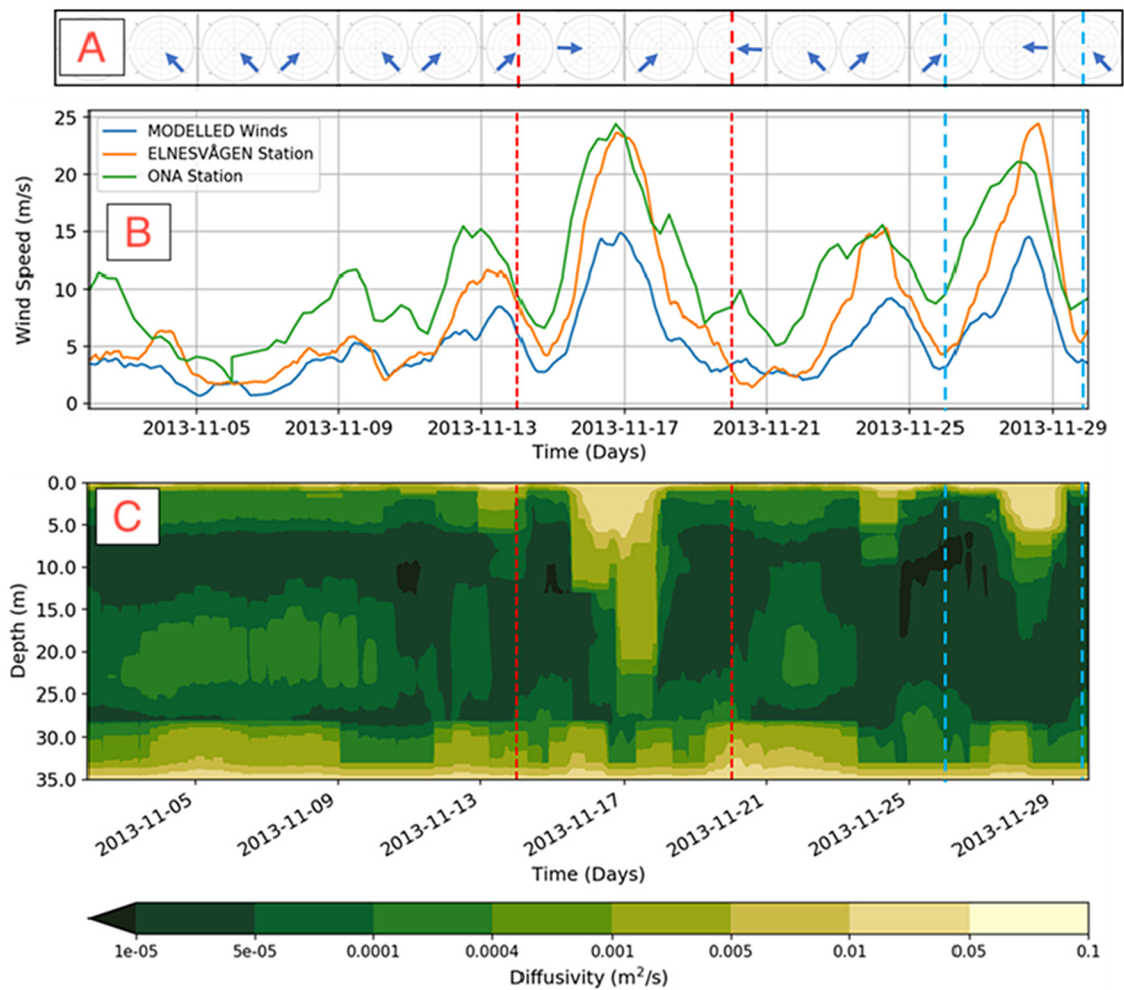
Fig. 6. Time series of wind speed (B) and vertical diffusivity of water column near the discharge points in Frænfjorden (C) during November 2013. The upper row (A) contains arrows showing main wind direction during November 2013. The vertical red and blue dashed lines delineate two different strong wind events. In panel B, the green line shows 6-hourly data from Norwegian Meteorological Institute observation point 62480 (ONA Station, located approximately 30 km west of the STP). The orange line shows 20-minute data from a roof-mounted station at Omya Hustadmarmor AS (ELNESVÅGEN Station), and the blue line shows 3-hourly modelled data (MODELLED winds). A 24-h rolling mean has been applied to these data. (For interpretation of the references to colour in this figure legend, the reader is referred to the web version of this article.)

3.3. Current predictions compared to measurements

A time series of current speed for November 2013 (Fig. 7) shows how the variations in modelled current speed compare to observations. At station S14, the model responds to the high current events seen in measurements. The average current speed agrees well at 11 m, while the model underestimates current speed at 27.5 m. At station S38, current speeds are generally low both in the model and observations, and at station S40, the model agrees fairly well with measurements both at 11 and 27.5 m. At the easternmost station, SB4, current speeds are low, and the model tends to overestimate the tidal current speed.

The time series for station S14 shows the model responding more clearly to the strong wind event in November 2013 at 11 m than at 27.5 m, while measurements show a clear effect at both depths. This may be caused by inaccuracy in the estimate of wind stress on the water column in SINMOD, as it was previously seen that the modelled wind did not reach the same high speed as the measured wind (see Fig. 6).

The current statistics for station S14 at 27.5 m (Fig. 8) show two clearly dominant directions (northeast and southwest) in the model, while the observations show current directions fairly evenly distributed from north-east to south-west via the south-east quadrant. For station S40 at 27.5 m (Fig. 9), both the model

and the observations show clearly dominant directions (northeast and southwest), although there is more spread in the observations.

The distribution of current speeds and directions agree quite well between model and observations at station S40 at 27.5 m (Fig. 9), while at station S14 at 27.5 m (Fig. 8) the model underestimates current speeds and produces significantly less spread in directions. It is common to observe greater spread in measurements than in model results, as seen for S40, due to both measurement noise and small scale variability in the currents that are not represented by the model. The deviations at S14 are likely to be caused by local bathymetric conditions. The station is located near a ridge on the north side, which may induce bathymetric control of the current, both leading to increased current speeds and pushing currents southwards. As the ridge is not satisfactorily represented near the measurement point in the numerical model, this is consistent with the deviations seen in Fig. 8.

It should be noted that there are no sampling stations for currents inside the STP area, only at or outside the border, with the nearest station located more than 1 km away, and this limits our ability to check the model predictions close to the particle release. On the other hand, the modelled bathymetry in the
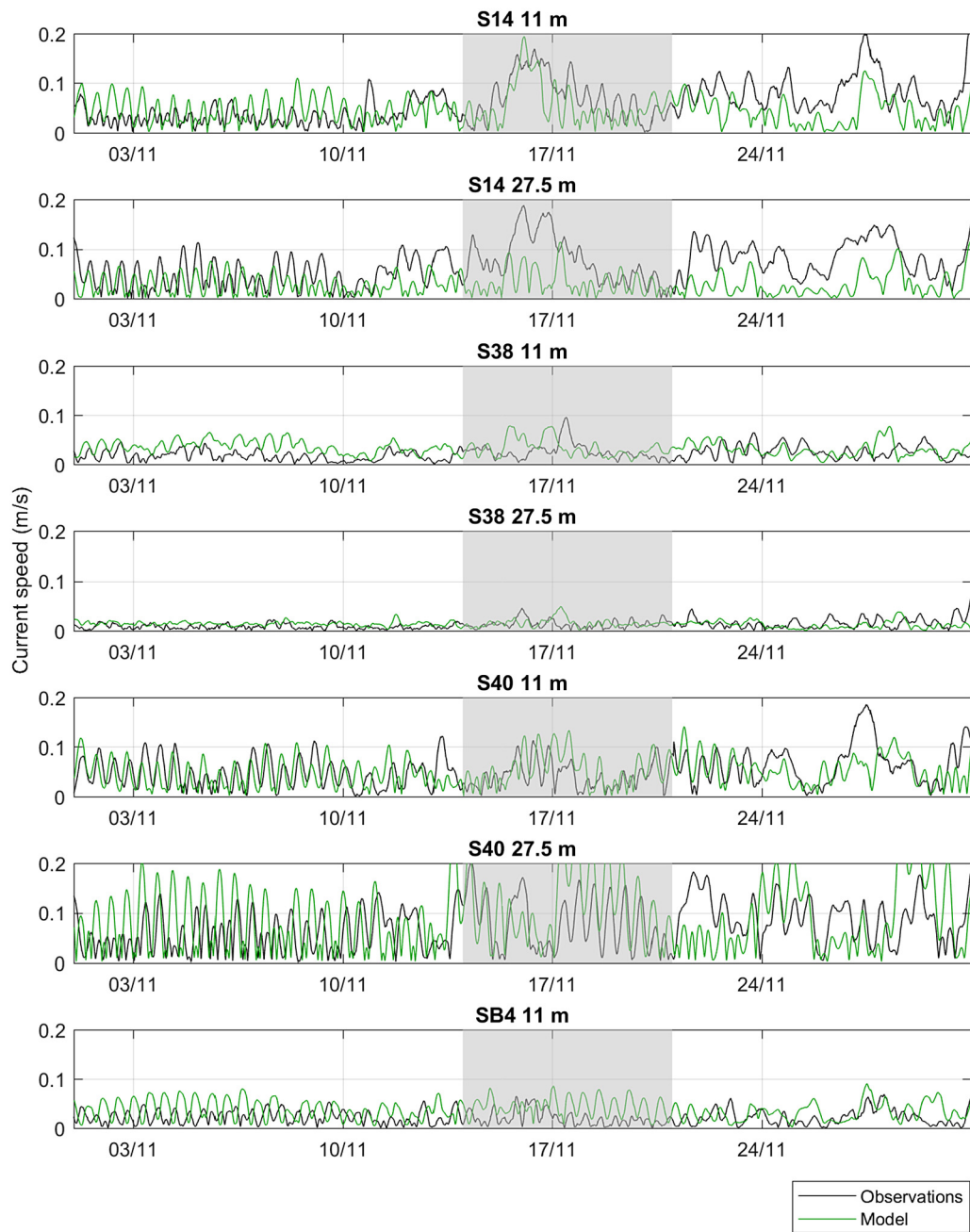
Fig. 7. Comparison of observed and modelled current speed in November 2013 at four stations. Both model and observation time series are 4 h running means of the current speed.

deposit area is based on recent high resolution measurements, which improves the ability of the model to accurately represent currents in the area.

### 3.4. Predicted tailings concentration compared to measured turbidity

Prediction of suspended tailings concentration from the transport model was compared to turbidity measurements at four different stations for November 2013, shown in Fig. 10. A rolling 24 h mean was applied to both turbidity and concentration time series, to highlight trends beyond tidal variations. We lacked site-specific calibration of the turbidity data, and thus concentration values could not be explicitly calculated from turbidity, nor absolute levels easily compared. In addition, the model predicts

concentrations of tailings from the discharge, whereas the turbidity includes also contributions from other sources (background), which may vary over time. However, by comparing relative increases and changes in the two signals, a useful semi-quantitative comparison and evaluation of the model performance could still be made.

As previously mentioned, there was a strong wind event around November 17 (see Fig. 6). In Fig. 10, modelled sediment concentration and measured turbidity are shown for four different stations for all of November 2013. The signature of the increased mixing during this strong wind event is clearly present in the elevated turbidity signal at station SB4, and well matched by increases in the model predictions levels. The RTbuoy station signal also has an increase during this period, matched by the model, but it is less distinct from the rest of the period, whereas
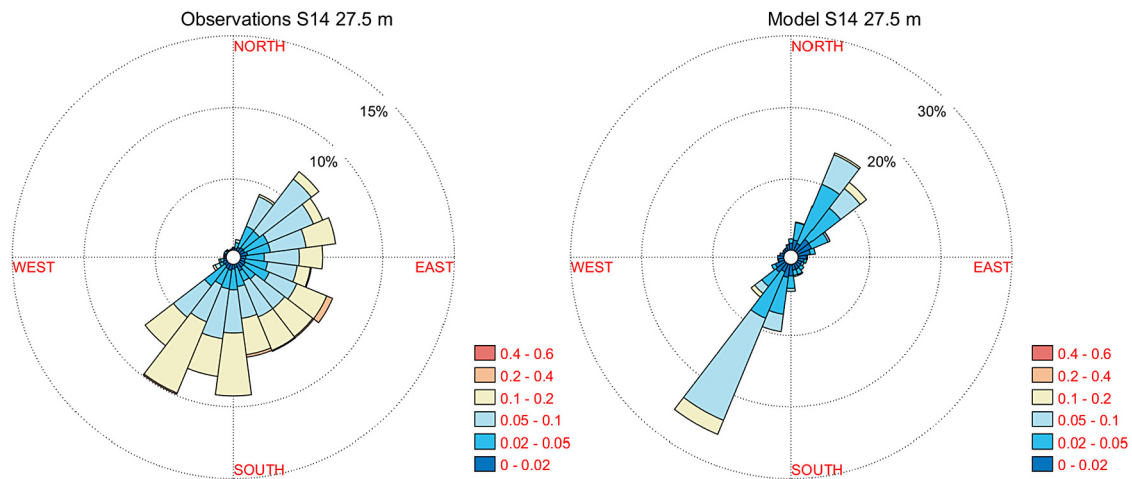
Fig. 8. Comparison of observed and modelled current statistics for November 2013 at station S14 at 27.5 m. Both model and observation data was filtered with 1 h running means to reduce noise. Note that the plots have different radial axes to enhance readability.
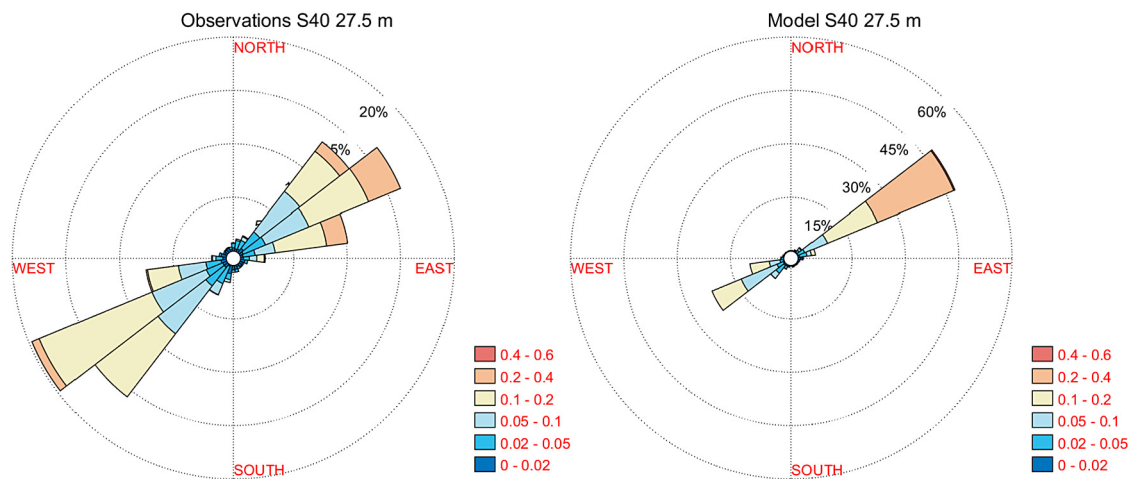
Fig. 9. Comparison of observed and modelled current statistics for November 2013 at station S40 at 27.5 m. Both model and observation data was filtered with 1 h running means to reduce noise. Note that the plots have different radial axes to enhance readability.

at station S38 there is little increase in either turbidity or model predicted concentration. Station S14 has a marked increase in the model suspended sediment concentration during the wind event around November 17, but less so in the measured turbidity. Later in the month there are two fairly distinct peaks present in both signals, though stronger in the turbidity.

During the strong wind event at November 17, the model predictions of suspended sediment concentration show some interesting similarity with the turbidity signals. The correlation is particularly strong at stations SB4 and RTbuoy, where both signals show distinct peaks. At station S38, there is little response in either signal, indicating that the model correctly predicts little or no additional sediment transport in the direction of this station. The profiling buoy (RTbuoy) data obtains information on turbidity as both a function of depth and time, and this is presented in Fig. 11 (lower panel) together with model predictions from the same area (upper panel). During the strong wind event, both the measured turbidity and the model indicate mixing upwards in the water column, visible as elevated turbidity/concentration through the entire water column. This is in contrast to the rest of the period, where there is little mixing above 20 m (15 m) in the turbidity (model) signals.

For station S14, the correlation between the model and the measured turbidity is not particularly good during the strong

wind event (though it is better later in the month). Current speed and direction are naturally a very strong driver for predicted sediment concentration at different locations, and in Fig. 8, we observe that the measured currents at station S14 have more spread in direction than the hydrodynamic model predicts, as discussed in the previous section. This discrepancy would explain the sometimes poor correlation between measured turbidity and modelled suspended sediment concentration.

3.5. Tailings transport during a strong wind event

During the strong wind event around November 17, 2013 (see Sections 3.2 and 3.4), the model predicts increased concentrations at some of the turbidity measurement stations, consistent with observations. To investigate this event more closely, we calculated daily mean values of the predicted suspended tailings concentration, matching the local tidal cycles, shown in Fig. 12. The left column shows depth-maximum concentrations, while the right column shows a depth-easting projection, with maximum values selected along the northing direction. The rows represent 24 h periods immediately preceding the wind event (top row), during maximum (upper middle row) and after (lower middle row). For comparison, the bottom row shows the situation during the second strong wind event (November 28), when the wind directions were different.
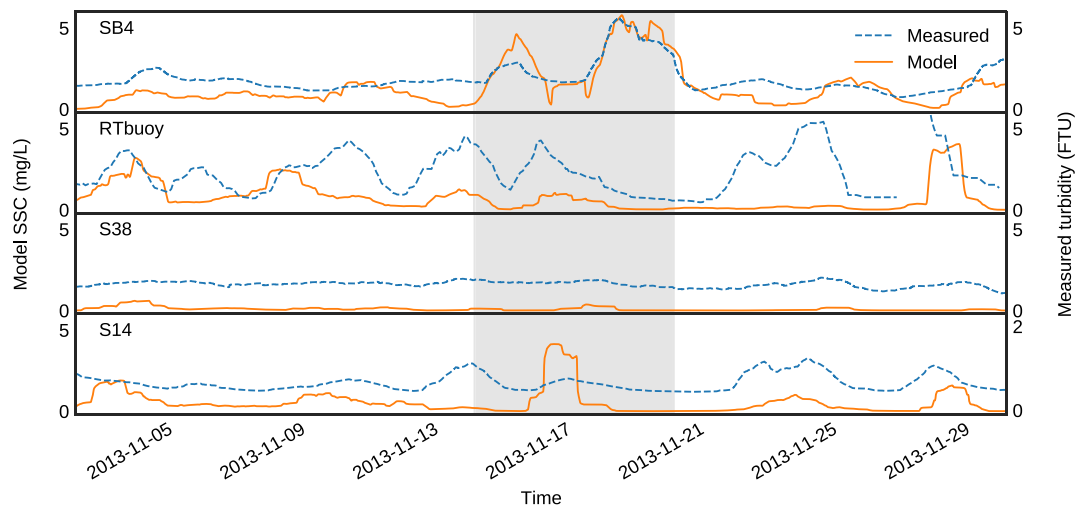
Fig. 10. Model predictions for suspended solid concentrations (mg/L, left axis, full orange lines) and measured turbidity at different station locations (FTU, right axis, blue dashed lines). Note that the bottom panel uses a different range of turbidity values than the others. The shaded grey area delineates a strong wind event. See text for discussion. (For interpretation of the references to colour in this figure legend, the reader is referred to the web version of this article.)
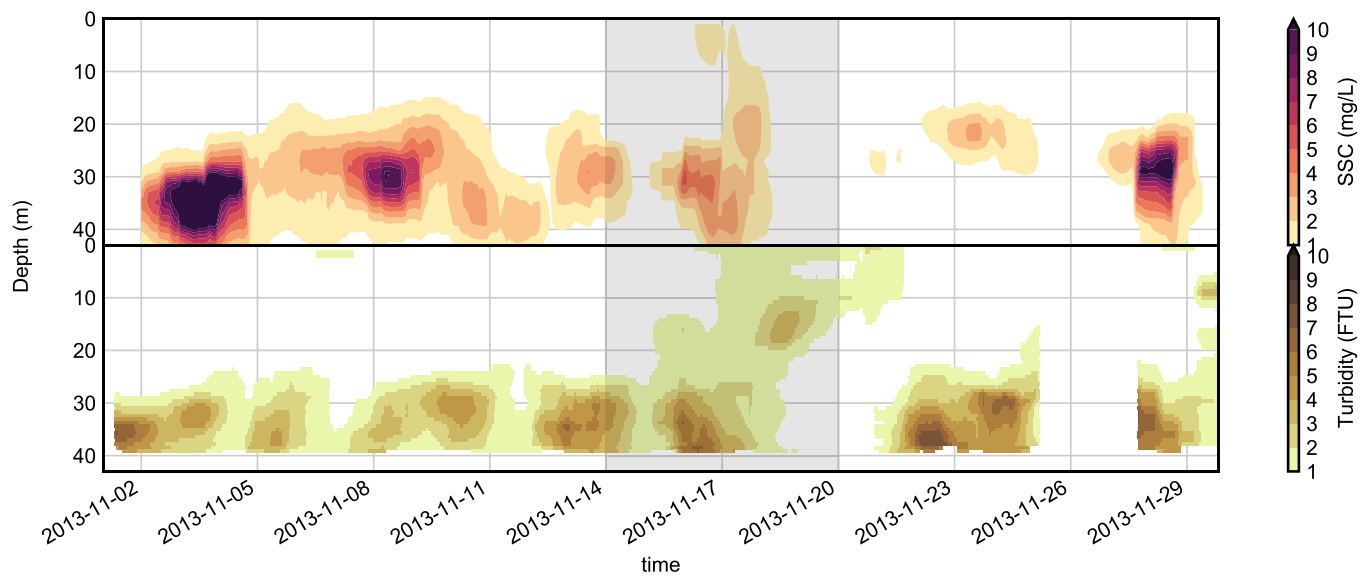
Fig. 11. Model predictions for suspended solid concentration (mg/L, top panel) and measured turbidity at profiling real-time buoy location (FTU, bottom panel). The shaded area delineates a strong wind event.

The strong winds clearly have an effect on the horizontal spreading and vertical mixing of the tailings, with a larger area (volume) having increased concentration during maximum wind compared to before or after. There is also more upward mixing, with concentrations exceeding 1 mg/L found throughout the upper 20 m of the water column in the area around the real-time buoy (diamond marker), consistent with observations as shown above. In contrast, during the second wind event with a different wind direction (bottom row), mean concentrations remain largely below 1 mg/L in the upper 20 m, and the horizontal spreading is less than during the wind event on November 17.

A more summarised view of the spreading is obtained by calculating the total amount of tailings in suspension outside the main STP area (region indicated in Fig. 1), as well as the volume of water exceeding 1 mg/L outside the STP area. This is shown in Fig. 13, and the strong wind period is indicated by the grey shading. Strong (semi-)diurnal tidal variations in these signals are observed, as well as longer cycles, but the wind effect can also clearly be seen in the signal increase around November 17, with

increased export of tailings from the main STP area. The later strong wind event (around November 28) has a lower signature due to the difference in direction, as previously discussed.

3.6. Tailings sedimentation

Predicted time-averaged sedimentation rate of tailings on the sea bed (mm/y) is shown in Fig. 14, based on a 6-month simulation of continuous discharge (June to November 2013), with 48 h binned average discharge rates. While the most intense deposition occurs close to the discharge points, we observe some asymmetry about these points, with a tail of relatively higher rates extending eastwards. There is also some sedimentation on the western slope and in the deeper part to the west, but outside the main STP area the deposition rates are lower, and less than 5 mm/y, except for in a transition zone near the STP border. Some sedimentation (< 2 mm/y) occurs for several kilometres west from the western discharge point, falling below 0.1 mm/y beyond station S40.
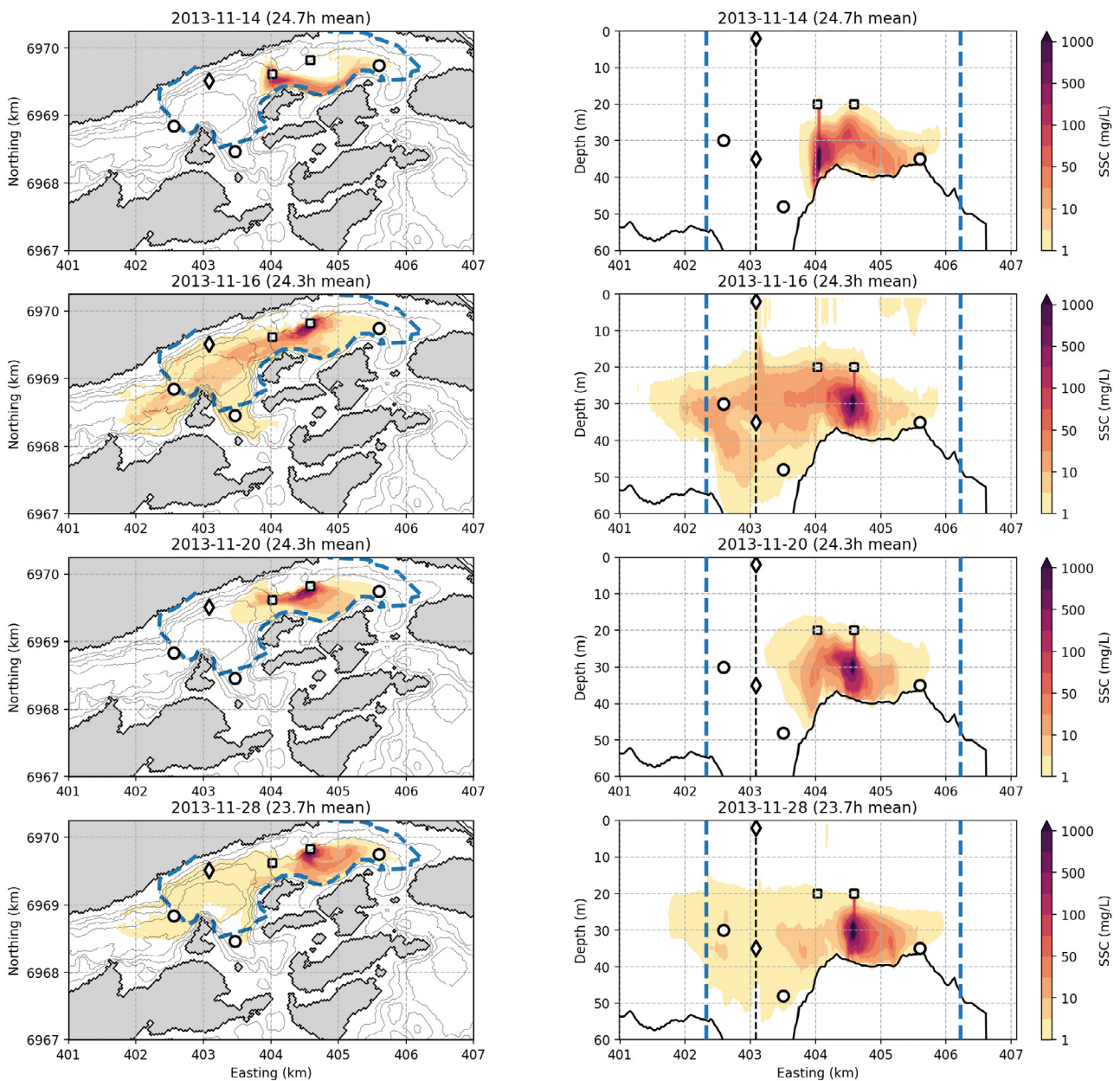
Fig. 12. Suspended tailings concentration averaged over two tidal cycles (approximately 24 h) for three time windows: before (top), during (middle) and after (second middle) the major wind event. The bottom rows shows mean concentrations during the second wind event on November 28, for comparison. The left column shows depth-maximum values, while the right column shows values with the maximum taken in north–south direction (depth-easting, approximately along-fjord). Measurement station locations are shown as black circles, discharge points as black squares, while the black diamond is the location of the real-time buoy. The STP area is indicated by the blue dashed lines.

Sediment trap data at several stations for the period in question was collected during routine monitoring, which provide us with some additional opportunity for assessing the model predictions. The station positions are labelled in Fig. 14, and the reported values are shown in Fig. 15, together with model predictions. The error bars on the measurements are estimates based on uncertainties in the determination of the tailings content of the collected sediments. We extracted rates for 3 × 3 grid cells centred on the station coordinates, which is used to calculate the model spatial variability in the immediate area of each station, represented by the box plots. Both model and measurements show a trend of decreasing sedimentation rate with distance from the discharge points, but also the east–west asymmetry, with the eastern station (SB4) having somewhat elevated rate compared to station S38. The spatial variability in the model predictions are

also greater at SB4. This station is closer than the others to the eastern pipe outlet, which could contribute to the variability here.

The model predictions, although correlating well with the measurements, are generally lower in value. However, there is significant spatial variability, especially at station SB4, and at station S40 there is a small area of elevated sedimentation nearby (> 1 mm/y) (see Fig. 14). In the presence of such variability, and considering that the transport model prediction are made on 30 m (horizontal) grid cells, a very close agreement with measurements cannot be expected. If a set of sediment traps were deployed in a close grid layout, the true variability could potentially be determined; unfortunately, the available dataset does not permit such a determination. The present model simulation also does not account for the effect of resuspension, which may have contributed additionally to the measured levels in the
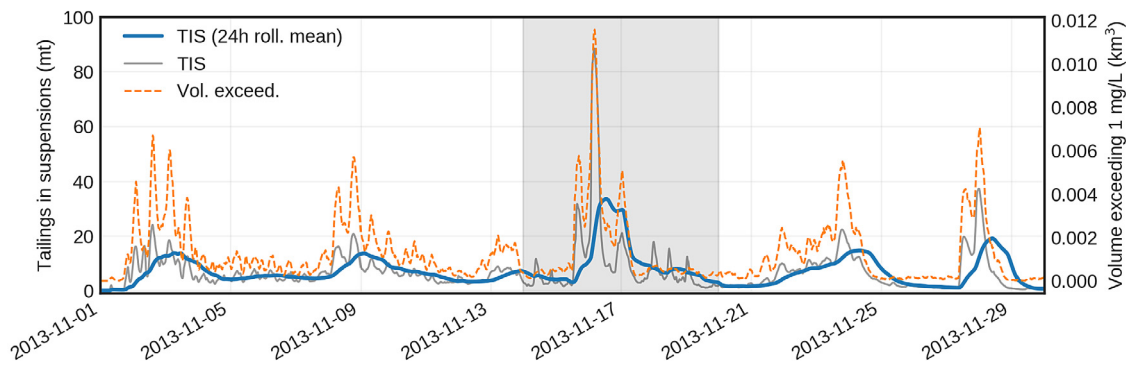
Fig. 13. Model predictions of total tailings in suspension (TIS) outside the STP area (metric tonnes, grey and blue thick line), and volume exceeding 1 mg/L outside the STP area (orange dashed line).
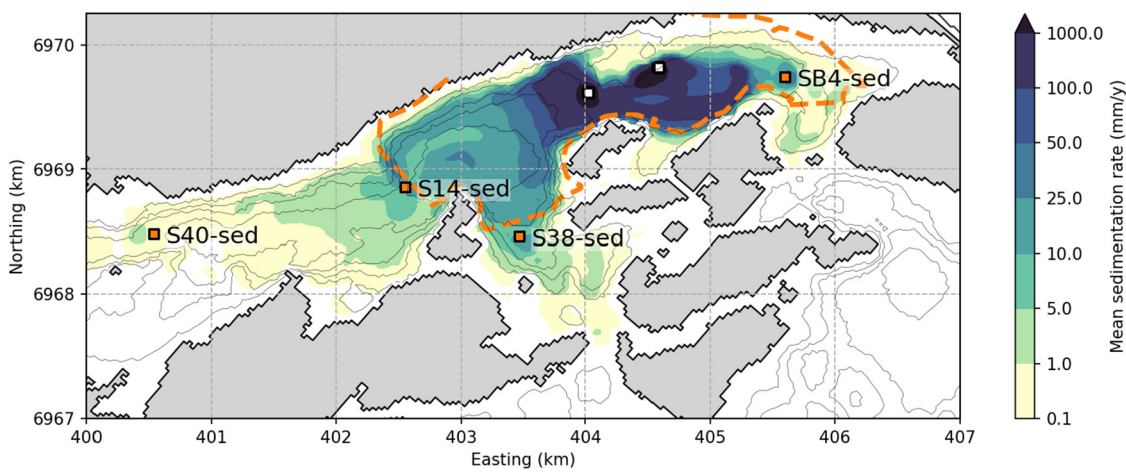
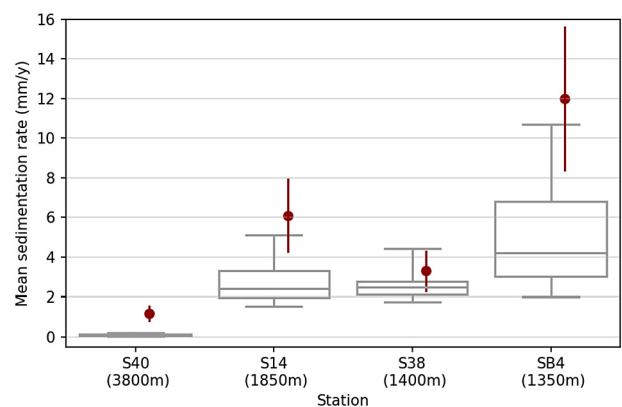**Fig. 14.** Mean sedimentation rate calculated from a 6 month simulated discharge period (June–November 2013).

sediment traps. Thus, we consider the model results in reasonable agreement with the measurement.

4. Summary and conclusion

Simulations of mine tailings particulate dispersion from a submarine tailings placement (STP) located in Frænfjorden (western Norway) were carried out using a suite of three-dimensional models that includes high-resolution wind, hydrodynamics and particle transport. The simulations were designed to calculate suspended tailings concentrations and dispersion based on new capabilities included in the DREAM model.

Suspended tailings concentrations are highly dynamic in the STP area, and its transport is accomplished predominately by the tidal- and wind-driven currents as well as other exchange processes with coastal waters adjacent to the fjord. Strong wind events during November 2013 caused an increase in both suspended tailings concentration levels and influence area, as well as the elevated export rate of tailings from the inner STP area.

The model results generally show a fair agreement with observations. Comparisons between observations and modelled winds showed a good temporal correlation with some underprediction of absolute values. Direct comparisons with ADCP measurements indicated that modelled currents have a high agreement in some

Fig. 15. Distribution of mean tailings sedimentation rate (box plots), calculated from a simulated 6 months of discharge (June–November 2013), at four different stations (see map in Fig. 14). Estimates based on sediment trap measurements are also shown (red dots and lines). The distances from each station to the western discharge point are indicated.

stations and some deviations in other stations. These deviations can be explained by bathymetric details not resolved in the

model, which may affect the local flow. Measurements of turbidity were found to be in qualitative agreement with predicted suspended tailings concentrations. Comparisons between sediment trap data and predicted sedimentation rates showed some underpredictions in absolute values, but the overall observed pattern is also found in the model output.

The simulations were designed to identify the tailings transport, and new capabilities of the model to include the effect of flocculation were essential to predict their distribution in the fjord basin. Mean tailings sedimentation rates in the fjord basin, predicted by the model, provide some insight into the potential environmental footprint of the discharge and may be useful for future optimisation of the discharge itself.

CRediT authorship contribution statement

Raymond Nepstad: Conceptualization, Methodology, Software, Investigation, Data curation, Writing - original draft, Writing - review & editing, Visualization, Project administration, Funding acquisition. **Maria Liste:** Conceptualization, Methodology, Data curation, Writing - original draft, Writing - review & editing, Visualization. **Morten O. Alver:** Investigation, Writing - review & editing, Visualization. **Tor Nordam:** Conceptualization, Writing - review & editing. **Emlyn Davies:** Conceptualization, Writing - review & editing. **Tormod Glette:** Investigation, Writing - review & editing.

Declaration of competing interest

The authors declare that they have no known competing financial interests or personal relationships that could have appeared to influence the work reported in this paper.

Acknowledgements

References

Alver, Morten, Michelsen, Finn Are, Knutsen, Øyvind, McClimans, Thomas, 2016. Current Conditions in Frænfjorden. Technical report, SINTEF Fisheries and Aquaculture.

Amante, Christopher, Eakins, Barry W., 2009. ETOPO1 Arc-Minute Global Relief Model: Procedures, Data Sources and Analysis. Technical report.

Aure, Jan, Strand, Øivind, Erga, Svein R., Strohmeier, Tore, 2007. Primary production enhancement by artificial upwelling in a western Norwegian fjord. Mar. Ecol. Prog. Ser. 352, 39–52.

Chowdhury, Mijanur R., Testik, Firat Y., 2014. A review of gravity currents formed by submerged single-port discharges in inland and coastal waters. Environ. Fluid Mech. 14 (2), 265–293.

Davies, Emlyn J., Nepstad, Raymond, 2017. In situ characterisation of complex suspended particulates surrounding an active submarine tailings placement site in a Norwegian fjord. Reg. Stud. Mar. Sci. 16, 198–207.

Davies, H.C., Turner, R.E., 1977. Updating prediction models by dynamical relaxation: an examination of the technique. Q. J. R. Meteorol. Soc. 103, 225–245.

Dold, Bernhard, Bernhard, 2014. Submarine tailings disposal (STD) - A review. Minerals 4, 642–666.

Dyer, K.R., 1989. Sediment processes in estuaries: future research requirements. J. Geophys. Res.: Oceans 94 (C10), 14327–14339.

Egbert, Gary D., Erofeeva, Svetlana Y., 2002. Efficient inverse modeling of barotropic ocean tides. J. Atmos. Ocean. Technol. 19 (2), 183–204.

Farkas, Julia, Altin, Dag, Hammer, Karen M., Hellstrøm, Kaja C., Booth, Andy M., Hansen, Bjørn H., 2017. Characterisation of fine-grained tailings from a marble processing plant and their acute effects on the copepod Calanus finmarchicus. Chemosphere 169, 700–708.

Farmer, David M., Freeland, Howard J., 1983. The physical oceanography of Fjords. Prog. Oceanogr. 12 (2), 147–219.

Findikakis, Angelos N., Law, Adrian W.K., 1998. Marine tailings disposal simulation. J. Hydraul. Eng. 124 (4), 370–383.

Glette, Tormod, 2014. Strøm og Partikkelmålinger i Frænfjorden 2013/2014. Technical report, DNV GL.

Hill, Paul S., Milligan, Timothy G., Geyer, W. Rockwell, 2000. Controls on effective settling velocity of suspended sediment in the Eel River flood plume. Cont. Shelf Res. 20 (16), 2095–2111.

Huang, Jianchun, Hilldale, R.C., Greimann, B.P., 2006. Cohesive sediment transport. In: Erosion and Sedimentation Manual. US Department of the Interior, Bureau of Reclamation Denver, pp. 4.1–4.46.

Jakobsson, Martin, Mayer, Larry, Coakley, Bernard, Dowdeswell, Julian A., Forbes, Steve, Fridman, Boris, Hodnesdal, Hanne, Noormets, Riko, Pedersen, Richard, Rebesco, Michele, et al., 2012. The international bathymetric chart of the Arctic Ocean (IBCAO) version 3.0. Geophys. Res. Lett. 39 (12).

Jensen, Tor, Hylland, Ketil, 2019. Environmental adaptive management: application on submarine mine tailings disposal. Integr. Environ. Assess. Manage. 15 (4), 575–583.

Johansen, Øistein, 2000. DeepBlow – a Lagrangian plume model for deep water blowouts. Spill Sci. Technol. Bull. 6 (2), 103–111.

Johansen, Øistein, Durgut, Ismail, 2006. Implementation of the Near-Field Module in the ERMS Model. Technical report, SINTEF Materials and Chemistry, URL www.sintef.no/globalassets/project/erms/reports/erms-report-no-23_near-field-module.pdf. ERMS Report No. 23.

Krone, R.B., 1963. A Study of Rheologic Properties of Estuarial Sediments. Technical report, pp. 1–41.

Kvassnes, Astri Jæger Sweetman, Iversen, Eigil, 2013. Waste sites from mines in Norwegian fjords. Mineralproduksjon 3, A27–A38.

Lee, Joseph H.W., Cheung, Valiant, 1990. Generalized Lagrangian model for buoyant jets in current. J. Environ. Eng. 116 (6), 1085–1106.

Lee, Byung Joon, Fettweis, Michael, Toorman, Erik, Molz, Fred J., 2012. Multimodality of a particle size distribution of cohesive suspended particulate matters in a coastal zone. J. Geophys. Res.: Oceans 117 (3).

Lepland, Aivo, Plassen, Liv, Schønenberger, Jasmin, Klug, Martin, Baeten, Nicole J., Chand, Shyam, Bøe, Reidulv, Bellec, Valérie Karin, Sandøy, Roar, Longva, Oddvar, 2019. Marine mine tailings disposal at Lillebukt, Stjernsundet, North Norway: distribution, sedimentary processes and depositional impacts. Nor. J. Geol. 98 (4), 461–482.

Mevenkamp, Lisa, Stratmann, Tanja, Guilini, Katja, Moodley, Leon, Oevelen, Dick van, Vanreusel, Ann, Westerlund, Stig, Sweetman, Andrew K., 2017. Impaired short-term functioning of a benthic community from a deep norwegian fjord following deposition of mine tailings and sediments. Front. Mar. Sci. 4, 169.

Miljødirektoratet, 2015. Tillatelse til Virksomhet Etter Forurensningsloven for Omya Hustadmarmor AS. Tillatelsesnummer 2013/3358. Technical report.

Morello, Elisabetta B., Haywood, Michael D.E., Brewer, David T., Apte, Simon C., Asmund, Gert, Kwong, Y.T. John, Dennis, Darren, 2016. The ecological impacts of submarine tailings placement. In: Hughes, R.N., Hughes, D.J., Smith, I.P., Dal, A.C (Eds.), Oceanography and Marine Biology: An Annual Review, Vol. 54. pp. 315–366.

Myksvoll, M.S., Sandvik, A.D., Skarðhamar, J., Sundby, S., 2012. Importance of high resolution wind forcing on eddy activity and particle dispersion in a norwegian fjord. Estuar. Coast. Shelf Sci. 113, 293–304.

Neumeier, Urs, Ferrarin, Christian, Amos, Carl L., Umgiesser, Georg, Li, Michael Z., 2008. Sedtrans05: An improved sediment-transport model for continental shelves and coastal waters with a new algorithm for cohesive sediments. Comput. Geosci. 34, 1223–1242.

Ramirez-Llodra, Eva, Trannum, Hilde C., Evenset, Anita, Levin, Lisa A., Anderson, Malin, Finne, Tor E., Hilario, Ana, Flem, Belinda, Christensen, Guttorm, Schaanning, Morten, Vanreusel, Ann, 2015. Submarine and deep-sea mine tailing placements: A review of current practices, environmental issues, natural analogs and knowledge gaps in Norway and internationally. Mar. Pollut. Bull. 97, 13–35.

Reed, Mark, Hetland, Ben, 2002. DREAM: a dose-related exposure assessment model technical description of physical-chemical fates components. In: Proceedings of SPE International Conference on Health, Safety and Environment in Oil and Gas Exploration and Production.

Rye, Henrik, Reed, Mark, Ekrol, Narve, 1998. The PARTRACK model for calculation of the spreading and deposition of drilling mud, chemicals and drill cuttings. Environ. Model. Softw. 13 (5–6), 431–441.

Rye, Henrik, Reed, Mark, Frost, Tone K., Røe Utvik, Toril I., 2004. Comparison of the ParTrack mud/cuttings release model with field data. Environ. Model. Softw. 19 (7–8), 701–716.

Rye, Henrik, Reed, Mark, Frost, Tone Karin, Smit, Mathijs G D, Durgut, Ismail, Johansen, Øistein, Ditlevsen, May Kristin, 2008. Development of a numerical model for calculating exposure to toxic and nontoxic stressors in the water column and sediment from drilling discharges. Integr. Environ. Assess. Manage. 4 (2), 194–203.

Skamarock, W.C., Klemp, J.B., Dudhia, J., Gill, D.O., Barker, D.M., Duda, M.G., Huang, X.-Y., Wang, W., Powers, Jordan G., 2008. Technical report, NCAR.

Skei, Jens M., 2013. The dilemma of waste management in the mining industry – criteria for sea disposal. Mineralproduksjon 3, 1–4.

Skei, Jens M., Syvitski, James P.M., 2013. Natural flocculation of mineral particles in seawater – influence on mine tailings sea disposal and particle dispersal. Mineralproduksjon 3, 1–10.

Slagstad, Dag, McClimans, Thomas A., 2005. Modeling the ecosystem dynamics of the Barents Sea including the marginal ice zone: I. Physical and chemical oceanography. J. Mar. Syst. 58 (1–2), 1–18.

Sternal, Beata, Junttila, Juho, Skirbekk, Kari, Forwick, Matthias, Carroll, Jo Lynn, Pedersen, Kristine Bondo, 2017. The impact of submarine copper mine tailing disposal from the 1970s on Repparfjorden, northern Norway. Mar. Pollut. Bull. 120 (1–2), 136–153.

Sundfjord, Arild, Ellingsen, Ingrid, Slagstad, Dag, Svendsen, Harald, 2008. Vertical mixing in the marginal ice zone of the northern barents sea, results from numerical model experiments. Deep Sea Res. II 55 (20), 2154–2168.

van Leussen, Wim, 1994. Estuarine Macroflocs and their Role in Fine-Grained Sediment Transport (Ph. D. Thesis). University of Utrecht.

van Sebille, Erik, Griffies, Stephen M., Abernathey, Ryan, Adams, Thomas P., Berloff, Pavel, Biastoch, Arne, Blanke, Bruno, Chassignet, Eric P., Cheng, Yu, Cotter, Colin J., Deleersnijder, Eric, Döös, Kristofer, Drake, Henri F., Drijfhout, Sybren, Gary, Stefan F., Heemink, Arnold W., Kjellsson, Joakim, Koszalka, Inga Monika, Lange, Michael, Lique, Camille, MacGilchrist, Graeme A., Marsh, Robert, Mayorga Adame, C. Gabriela, McAdam, Ronan, Nencioli, Francesco, Paris, Claire B., Piggott, Matthew D., Polton, Jeff A., Rühs, Siren, Shah, Syed H.A.M., Thomas, Matthew D., Wang, Jinbo, Wolfram, Phillip J., Zanna, Laure, Zika, Jan D., 2018. Lagrangian ocean analysis: Fundamentals and practices. Ocean Model. 121, 49–75.

Vare, L.L., Baker, M.C., Howe, J.A., Levin, L.L., Neira, C., Ramirez-Llodra, E.Z., Richelt-Brushett, A., Rowden, A.A., Shimmield, T.M., Simpson, S.L., Soto, E.H., 2018. Scientific considerations for the assessment and management of mine tailings disposal in the deep sea. Front. Mar. Sci. 5, 15.